Role of Aerosil Dispersion on the Activated Kinetics of the $LC_{1-x}Sil_x$ System

Dipti Sharma,*,† John C. MacDonald,‡ and Germano S. Iannacchione†

Department of Physics and the Department of Chemistry and Biochemistry, Worcester Polytechnic Institute, Worcester, Massachusetts 01609

Received: August 11, 2006; In Final Form: October 23, 2006

This study explores the role of aerosil dispersion on activated phase transitions of bulk octylcyanobiphenyl (8CB) liquid crystals by performing heating rate-dependent experiments. Differential scanning calorimetry (DSC) was used at various heating ramp rates in order to probe the activated phase dynamics of the system. The system, $LC_{1-x}Sil_x$, was prepared by mixing aerosil nanoparticles (7 nm in diameter) in the bulk 8CB by the solvent dispersion method (SDM). LC represents bulk 8CB, and Sil represents aerosil nanoparticles with concentration x in percent. The concentration of the aerosil nanoparticles (x) varied from 0 to 0.2 g/cm^3 in the bulk 8CB. Well-defined, endothermic peaks were found on a heating scan at melting and at the smectic-A to nematic (SmA−N) and nematic to isotropic (N−I) transitions. These peaks show a temperature shift and a change in their shapes and sizes in the presence of aerosil nanoparticles. In addition, an exothermic peak also appeared before the melting peak during the heating scan in the presence of aerosil nanoparticles. All transitions shifted significantly with different heating ramp rates, following an Arrhenius behavior, showing activated kinetics. The presence of aerosil nanoparticles caused a significant increase in the enthalpy and a decrease in the activation energy compared to the results found in bulk 8CB. This behavior can be explained by aerosil dispersion in the $LC_{1-x}Sil_x$, inducing a disorder in the bulk 8CB. Infrared (IR) spectroscopy shows a shift to higher frequency for the broad peak at 1082 cm^{-1}, corresponding to an Si−O bond as the density of the aerosil increases, and can be explained in terms of surface and molecular interactions between aerosil nanoparticles and 8CB liquid crystal molecules.

I. Introduction

Aerosil-dispersed, liquid crystal systems are particularly attractive materials for research to understand changes in the physical behavior of those systems caused by the random disorder introduced in the bulk liquid crystals. Many studies have been done on aerosil-dispersed systems so far.[1−11] These studies reported the direct correlation length, photopyroelectric studies reporting specific heat and conductivity, Raman scattering, and dielectric relaxation studies for different liquid crystal systems doped with aerosils. Liquid crystals in their pure form are prototypical research materials for fundamental studies and technical application,[12−17] where the presence of aerosil creates a disorder and brings changes in the behavior of the liquid crystals on a wider range and makes the liquid crystal more interesting for research and applications.

The aerosil-dispersed liquid crystal, octylcyanobiphenyl (8CB), has been studied using light scattering, X-ray diffraction, and calorimetry in order to understand smectic-A to nematic (SmA−N) and nematic to isotropic (N−I) transitions.[10,18,19] Variations in peak shape and size with changes in the aerosil density have been reported,[20−22] where AC calorimetry[22−25] has been used to explain the change in enthalpy, phase, and specific heat capacity of aerosil-dispersed, liquid crystal systems for smectic-A to nematic (SmA−N) and nematic to isotropic (N−I) transitions. Rate-dependent studies of these transitions of aerosil-dispersed liquid crystal, 8CB, have not been reported. Moreover, the heating rate effect on the melting transitions of these materials has yet to be investigated. Therefore, we have undertaken a detailed heating rate-dependent calorimetric study of a aerosil-dispersed, bulk 8CB liquid crystal system using differential scanning calorimetry (DSC) to show the activated rate kinetics of the various transitions of the system using Arrhenius theory. Here, DSC is a good tool and has been used to study rate kinetics of different research materials for a long time.[26−29] This study explores the effect of aerosil nanoparticles on the melting, SmA−N, and N−I transitions of the 8CB liquid crystal and gives information about molecular and surface interactions between aerosil nanoparticles and 8CB molecules based on data collected using infrared (IR) spectroscopy.

We report the rate-dependent study of the phase transitions of an aerosil-dispersed, liquid crystal system, $LC_{1-x}Sil_x$, using Arrhenius theory. Four different densities of the aerosil nanoparticles in 8CB were studied. The heating scans were performed at four different heating ramp rates using DSC to understand the rate kinetics of the transitions of the system. The surface interaction between aerosil nanoparticles and 8CB molecules also was observed using IR spectroscopy. Sample preparation, experimental procedure, and involved theory are described in section II. The results are shown in section III, with discussion and conclusions drawn in section IV.

II. Experimental Section

A. Sample Preparation. The system $LC_{1-x}Sil_x$, used in this study, was the nanocolloidal mixture of hydrophilic, type-300 aerosil nanoparticles in the bulk octylcyanobiphenyl 8CB liquid crystal. The specific surface area of a type-300 aerosil nanoparticle is 300 m^2 g^{-1},[30] and the diameter of aerosil nanoparticles is roughly 7 nm, whereas the length of 8CB molecules is 2 nm, and the width is 0.5 nm. The molecular weights of bulk 8CB

† Department of Physics.
‡ Department of Chemistry and Biochemistry.

10.1021/jp065209z CCC: $33.50
Published on Web 12/09/2006

and the aerosil nanoparticles (SiO_2) are $M_w = 291.44$ and 60.08 g mol^{-1}, respectively. The bulk 8CB and the aerosil nanoparticles were obtained from Frinton Laboratories. In the $LC_{1-x}Sil_x$ system, LC represents bulk 8CB, and Sil represents aerosil nanoparticles, where x is the mass fraction of the aerosil nanoparticle in the system. The density of the aerosil nanoparticles in the bulk 8CB was varied in four steps from 0 to 0.2 g/cm^3. The concentration, x, was 0, 0.05, 0.10, 0.15, and 0.20% in the 1% $LC_{1-x}Sil_x$ system, where $x = 0$ and $x = 1$ represent bulk 8CB and pure aerosil, respectively, and other values of x show different densities of aerosil in the system. These samples were degassed for about 1 h under a vacuum unit at room temperature, 293 K, and then used in DSC and IR studies.

The nanocolloidal mixture of hydrophilic, type-300 aerosil nanoparticles (7 nm in diameter) in bulk 8CB was prepared following the solvent dispersion method (SDM).[31,32] The hydrophilic nature of the aerosils allows the silica particles to weakly hydrogen-bond to each other and to form a gel in an organic solvent; however, the basic free-floating aerosil unit typically consists of several of these spheres fused together during the manufacturing process.[22] Each 8CB and Sil sample was created by mixing appropriate quantities of the liquid crystal and the aerosil together and by dissolving the resulting mixture in spectroscopic grade (low water content) acetone. The resulting solution was then dispersed using an ultrasonic bath for about 1 h. As the acetone evaporates from the mixture, a fractal-like gel forms through diffusion-limited aggregation. Crystallization of the LC host can severely disrupt the gel structure, and so care was taken to prevent any formation of the solid phase of the liquid crystal during the experiments. The samples were subsequently dried under vacuum for more than 2 h at an elevated temperature. This preparation method has been shown to produce uniform and reproducible dispersions.[22]

The 8CB liquid crystal used in this work is a well-studied prototypical rod-like molecule with a rigid biphenyl core at one end attached to an aliphatic tail, and the other end is attached to a polar, cyano group. The pure material undergoes a weak first-order isotropic to nematic transition at $T_{IN}^{o} = 313.98$ K, a continuous nematic to smectic-A transition at $T_{NA}^{o} = 306.97$ K, and crystallizes below 290 K,[33] as reported using the AC calorimetry technique at very slower ramp rates of 50 mK/h. The aerosil consists of SiO_2 (silica) spheres coated with (−OH) hydroxyl groups exposed on the surface. The hydroxyl groups on the surface enable the spheres to hydrogen-bond and form a thixotropic,[34] fractal gel in an organic medium such as 8CB.

The aerosil gel can be considered as randomly crossing, long silica chains with a very high pore volume fraction and no preferred orientation, as demonstrated previously by light scattering[35] and small-angle X-ray scattering (SAXS) studies.[22] These SAXS studies showed, however, that the basic aerosil unit generally consists of several of these spheres fused together during the manufacturing process.[22] The specific surface area of the type-300 aerosil is $a \approx 300$ m^2 g^{-1}, as determined by a Brunauer−Emmett−Teller (BET) adsorption isotherm and as specified by the manufacturer. The gelation threshold for the aerosil used in this experiment occurs approximately at a silica density of $\rho \approx 0.015$. Because of the surface hydroxyl groups, the polar 8CB molecules should anchor homeotropically at the silica surface. However, due to the short radius of curvature and the expected undulations of the silica surface, the actual surface orientation is most likely tilted.

The silica density dependence of the aerosil gel dynamics was studied in four dispersion samples of LC + aerosil, ranging from 0.05 to 0.20 g cm^{-3} (grams of silica per cm^3 of total volume). In addition, a pure aerosil gel sample of unknown density was also studied. All results were compared with the results of bulk 8CB, which we reported recently.[36]

B. Collection Of Data. *1. DSC.* For rate kinetics, the aerosil-dispersed 8CB system, $LC_{1-x}Sil_x$, was studied by differential scanning calorimetry (DSC) using a model MDSC 2920 calorimeter (TA Instruments). Four different densities of aerosil nanoparticles were studied in bulk 8CB. The lowest density, $x = 0.05\%$ (sample mass, 5 mg), was loaded into aluminum pans (dimensions, ∼8 mm diameter and ∼0.5 mm depth) placed into the DSC. DSC thermograms of the sample were obtained at heating scan rates of 20, 10, 5, and 1 K/min. The sample was quenched at 243 K and then kept isothermal for 10 min. The sample was then heated from 243 to 333 K at 20 K/min ramp rate and cooled to 243 K at the same ramp rate. The respective heat flow of the sample was recorded along with the temperature change during heating scans. The DSC thermograms showed endothermic peaks on heating scans at melting, SmA−N, and N−I transitions and also showed an additional exothermic peak before the melting transition. The sample was heated a second time, keeping experimental conditions the same. The results were identical for all transitions and confirmed that the phase transitions of the liquid crystal, aerosil-dispersed 8CB are reversible. Similar measurements were made at heating scan rates of 10, 5, and 1 K/min. Experimental and environmental conditions were kept identical for all runs so that a comparison of the phase transition parameters could be made to understand the effect of different heating rates on phase transitions of the sample. The DSC was well-calibrated at each scan rate. The above steps were repeated for other densities of the aerosil nanoparticles ($x = 0.10$, 0.15, and 0.20%) using the same procedure. The pure aerosil nanoparticle ($x = 1$) was also studied to compare the results with those from the bulk 8CB. The results of bulk 8CB are reported in our latest publication.[36] The temperature of the endothermic peaks is reported at the maximum height of the peaks instead of at the onset temperature because the temperature at the peak maxima reflects the maximum change in the enthalpy.

2. IR. A ThermoNicolet Nexus 670 FT-IR spectrometer equipped with an ATR accessory was used to study the interaction of 8CB with silica nanoparticles. A thin film of each sample with a varying density of the aerosil in the system ($x = 0$, 0.05, 0.10, 0.20, and 1) was loaded onto the ATR window, and the data were monitored. The results were plotted as percent reflectance versus wavenumber after subtracting the background for each sample.

C. Arrhenius Theory. Using Arrhenius theory,[37−40] the effective heating rate can be given by

$$\beta = \beta_o\left(\exp\left(\frac{-\Delta E}{RT}\right)\right) \tag{1}$$

where β is the effective heating rate in K/min, β_o is a constant in K/min, ΔE is the activation energy in J/mol, R is the universal gas constant in J/mol K, and T is the absolute temperature in K. This equation can also be shown as

$$\ln \beta = \ln \beta_o - \left(\frac{\Delta E}{RT}\right) \tag{2}$$

where ΔE is determined from the slope of the graph, which is plotted between $\ln \beta$ and $1/T$.

III. Results

A. Calorimetry: Kinetics. *1. Effect of Heating.* Figure 1 shows the results of the heating scan of the aerosil-dispersed

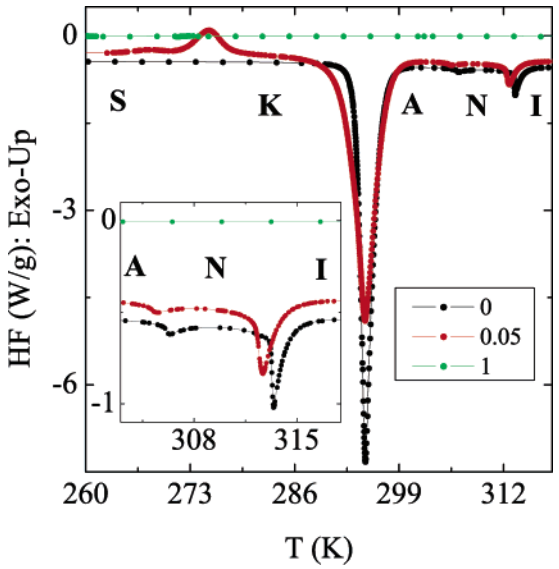

Figure 1. Heat flow (W/g) versus temperature (K) plot at a 10 K/min heating ramp rate for densities of $x = 0$, 0.05, and 1% in the $LC_{1-x}Sil_x$ system. The regions S, K, A, N, and I represent the solid, crystalline, smectic-A, nematic, and isotropic states of the aerosil-dispersed system, $LC_{1-x}Sil_x$, respectively. The inset figure shows the blow ups of the A, N, and I states of the system.

system $LC_{1-x}Sil_x$ at 10 K/min spanning the isotropic and crystal phases. The values of x are 0, 0.05, and 1%. They represent the results of the bulk 8CB, aerosil-dispersed 8CB with an aerosil density of 0.05 g/cm^3, and pure the aerosil without 8CB, respectively. On heating, as the temperature increases from 243 to 333 K, the aerosil-dispersed system shows an exothermic peak at 275.2 K (2.1 °C) as it moves from its solid state (S) to the crystalline state (K). It shows a nice and a little broader endothermic peak at the melting transition at 294.7 K as it moves further from the crystalline state (K) to the smectic-A (SmA) state. Further, it shows the smallest endothermic peak at 305.3 K from the smectic-A to nematic (SmA−N) transition, and at last, it shows an intermediate endothermic peak at 312.7 K from the nematic to isotropic (N−I) transition compared to the bulk 8CB results. In the presence of aerosil nanoparticles, all peaks show a little shift of 0.2−0.8 K toward a lower temperature from the position of the peaks found in bulk 8CB. The peak of each transition also changes in shape and size and becomes broader and smaller in the presence of aerosil nanoparticles. The exothermic peak appears only in the presence of the aerosil nanoparticle. The bulk 8CB shows the absence of an exothermic peak, and bulk aerosil nanoparticles show no peak on the heating scan. These results indicate that the presence of aerosil nanoparticles in the system changes the thermodynamics of the system.

2. Effect of Rate. A rate-dependent study of the $LC_{1-x}Sil_x$ system, for all densities of x, was also performed at different heating ramp rates of 20, 10, 5, and 1 K/min. Significant shifts in peak temperature toward a lower temperature were observed for all transitions for all densities of aerosil nanoparticles as the ramp rate decreased. Figure 2 shows the thermogram of the $LC_{0.95}Sil_{0.05}$ system at various heating ramp rates from 20−1 K/min. As ramp rate decreases, all transitions shift toward lower temperature. The rate of shifting in the melting (K−SmA) transition is more than that of the other SmA−N, N−I, or S−K transitions. To see clear shifts in each transition, the excess of specific heat capacity was plotted for each transition after subtracting the linear background. The excess specific heat

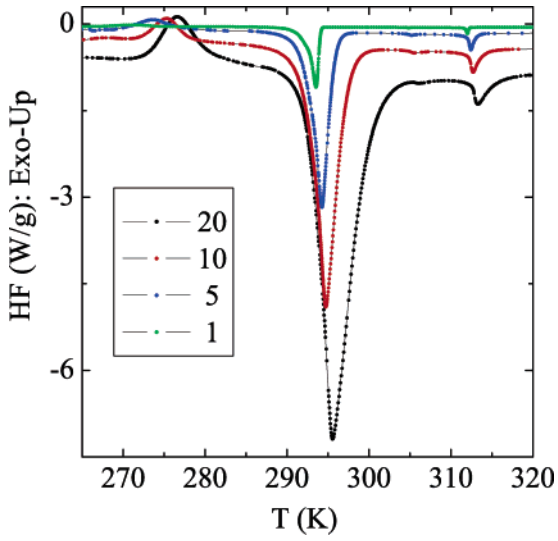

Figure 2. Rate effect on one density, $x = 0.05$, of the aerosil-dispersed system plotted as a heat flow (W/g) versus temperature (K) plot for a heating scan at different ramp rates from 20 to 1 K/min.

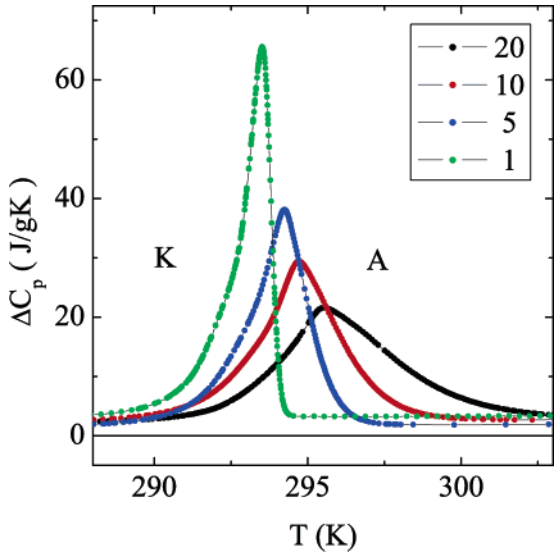

Figure 3. The excess of the specific heat capacity (J/g K) versus temperature (K) plot for the K−SmA transition, varying ramp rates from 20 to 1 K/min.

capacity for the system was obtained by subtracting a linear background from the specific heat, C_p, and is given as

$$\Delta C_p = C_p - C_p(\text{background}) \qquad (3)$$

where C_p(background) is the baseline and where C_p is the specific heat capacity of the sample. Figure 3 shows the excess of the specific heat capacity of the K−SmA transition at various ramp rates. It is clear that, as the ramp rate decreases, the peak becomes larger, sharper, and thinner, shifting toward a lower temperature and follows an Arrhenius behavior. The height range of the peak is found to be ∼20 to ∼60 J/g g KK. As shown in Figure 4, the peak for the N−I transition also becomes sharper and larger as the ramp rate decreases, but the height of the peak is intermediate and has the range of ∼2 to ∼6 J/g K. The SmA−N transition is the smallest transition and shows the smallest peaks with wings where the height range is ∼0.1 to ∼0.5 J/g K, as shown in Figure 5. The specific heat contribution of the SmA−N transition is obtained from ΔC_p by subtracting the heat capacity wing of the N−SmA transition

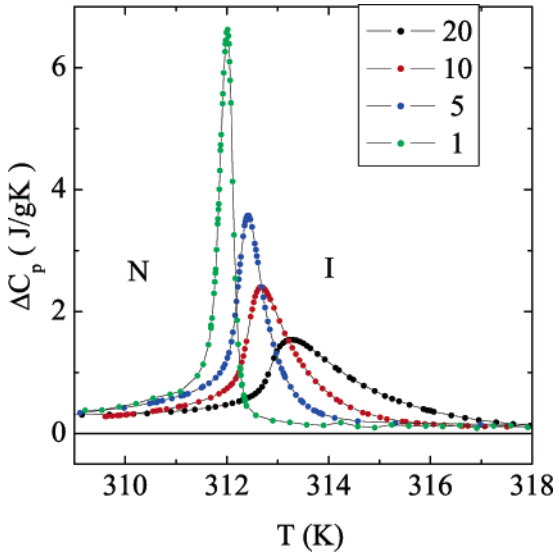

Figure 4. The excess of the specific heat capacity (J/g K) versus temperature (K) plot for the N−I transition, varying ramp rates from 20 to 1 K/min.

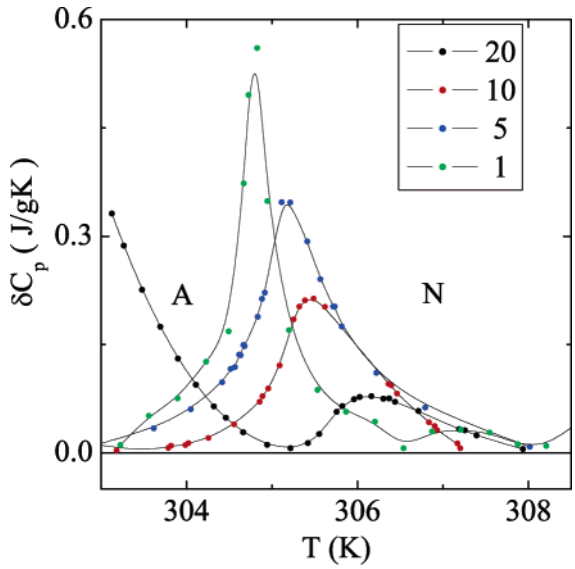

Figure 5. The excess of the specific heat capacity (J/g K) versus temperature (K) plot for the SmA−N transition, varying ramp rates from 20 to 1 K/min.

$$\delta C_p = \Delta C_p - \Delta C_p^{wing}(NA) \quad (4)$$

It is clear from Figure 5 that, as the ramp rate decreases, the peak gets bigger, sharper, and thinner, but the size of the peak is the smallest if compared with that of the other transitions. The peak shifts toward lower temperature with the decrease of the ramp rates, showing an Arrhenius behavior that indicates an activation energy for the transition.

Rate effects were also found for other densities of aerosil nanoparticles (x varies from 0.10 to 0.20) in the $LC_{1-x}Sil_x$ system. For simplicity, these plots are not shown here, but these results are considered in the data analysis. All transitions follow an Arrhenius behavior with different heating ramp rates and show rate-dependent kinetics. According to eq 2, when transitions were plotted as the ln of the heating rate versus the $1/T$ plot for all densities, all transitions show different activation energies. Figure 6 shows an Arrhenius plot for the K−SmA transition where the upper section shows lower densities of aerosil nanoparticles and where the lower section shows higher densities. The black dotted line shows the bulk 8CB results. The activation energy for the K−SmA transition can be calculated from the slope of the lines for all densities using eq 2. Similar plots are shown in Figure 7 for the N−I and in Figure 8 for the SmA−N transitions. Detailed results of the S−K transition will be discussed in our next paper.[41]

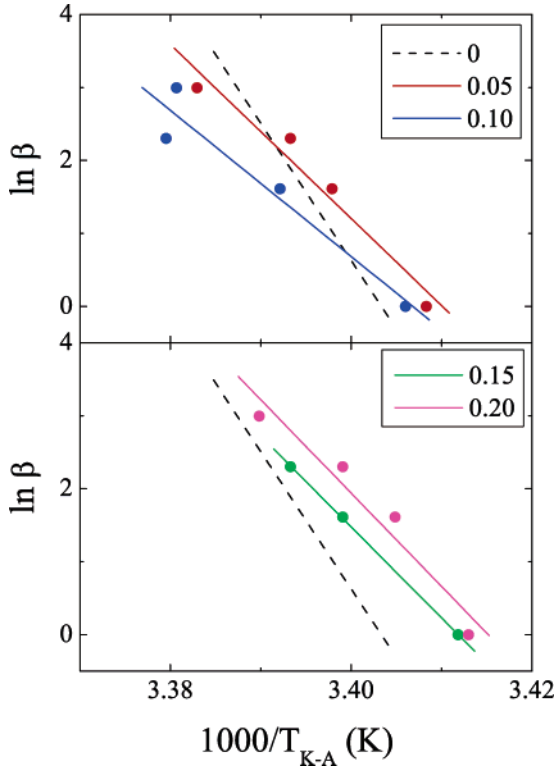

Figure 6. Arrhenius plot, ln β (K/min) versus $1/T$ (K) for the K−SmA transition for all densities. The upper plot shows lower densities, and the lower plot shows higher densities of aerosil. The dashed line shows the bulk 8CB. Smooth lines are the fits to the data points. Errors in $T_{K-A} \simeq \pm 0.05$ K.

The variation of the activation energy with a different density of the aerosil nanoparticles is shown in the Table 1 for each transition. The activation energy is minimum for the K−SmA transition and maximum for the SmA−N transition. As x percent increases, each transition shows a random pattern of variation of the activation energy.

3. Effect of Density. Figure 9 shows the density effect on the transitions of the $LC_{1-x}Sil_x$ system for all densities varying from 0 to 0.20 at a 5 K/min heating ramp rate. It is clear that, as the density increases, all transitions show a temperature shift in a random order, and peaks become smaller and broader for all transitions compared to bulk 8CB. To see clear density effect on the transitions, the excess of the specific heat capacity versus temperature was plotted for all transitions after subtracting a baseline. Figure 10 shows the blow up of the K−SmA transition. It is clear that, as the density increases, the peak first shifts toward a lower temperature, then moves toward a higher temperature, and again shifts back toward a lower temperature. The peak size becomes smaller, but wider, with the increase in the density. For the highest density, this transition shows a bump or multiple peaks that overlap. Figure 11 shows the blow up of the N−I transition. As the density increases, the peak shifts randomly toward lower, a little higher, and then lower temperatures but does not show changes as large as those of the K−SmA transition. The peak becomes smaller and broader as the density increases. The peak shifting for the SmA−N transition is shown in Figure 12. The interesting thing found in

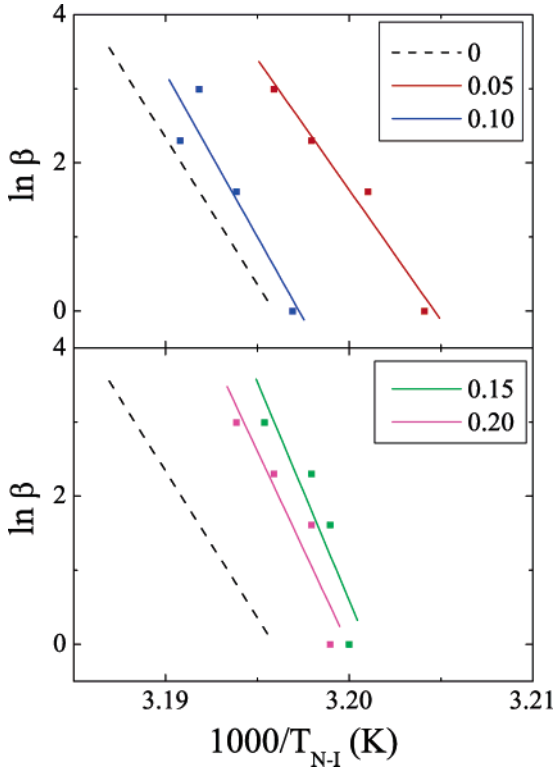

Figure 7. Arrhenius plot, ln β (K/min) versus $1/T$ (K) for the N−I transition for all densities. The upper plot shows lower densities, and the lower plot shows higher densities of aerosil. The dashed line shows the bulk 8CB. Smooth lines are the fits to the data points. Errors in $T_{N-I} \simeq \pm 0.01$ K.

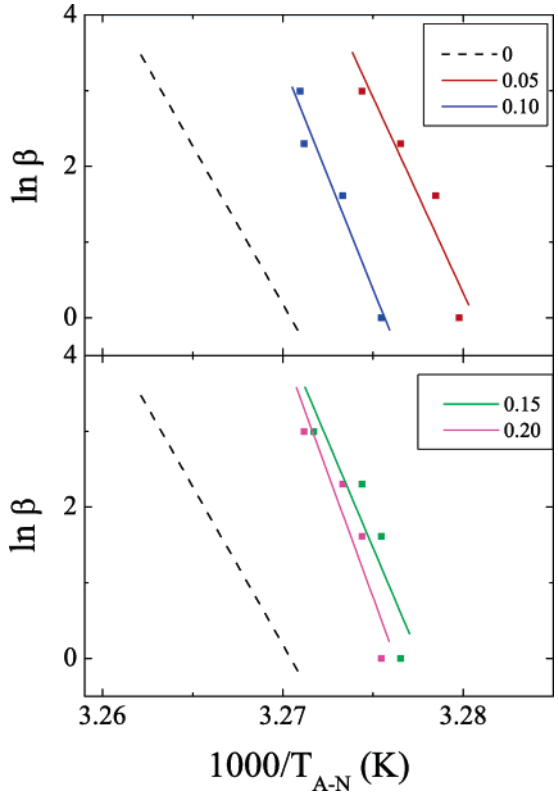

Figure 8. Arrhenius plot, ln β (K/min) versus $1/T$ (K) for the SmA−N transition for all densities. The upper plot shows lower densities, and the lower plot shows higher densities of aerosil. The dashed line shows the bulk 8CB. Smooth lines are the fits to the data points. Errors in $T_{A-N} \simeq \pm 0.01$ K.

Figures 10, 11, and 12 is the change in the enthalpy. As density increases, all transitions show a different pattern of enthalpy change. The details of the enthalpy change for each transition for all densities are shown in the Table 2. It is clear from the table that the K−SmA transition has a maximum enthalpy containing a maximum latent heat, whereas N−I has an intermediate enthalpy containing a minimum latent heat, and the SmA−N transition has a minimum enthalpy containing no latent heat. As the density increases, the enthalpy of the transitions increases following a random pattern. The maximum change in enthalpy is found for the K−SmA transition, and the minimum is for the SmA−N transition.

The change in the peak positions for all transitions as a function of density is shown in Figure 13. The peak positions were calculated for all densities after subtracting the value of the peak positions of the respective transitions found in bulk 8CB as $\Delta T(\mathrm{K}) = T(\rho_s) - T°$, where $T(\rho_s)$ represents the peak temperature of various transitions for different densities and where $T°$ represents bulk 8CB. The change in peak position found for the N−I and SmA−N transitions has been reported previously.[36] The variation found for the K−SmA transition is, however, completely unknown and unique to our study. As the density of the aerosil nanoparticles increases, peak positions as a function of temperature for each transition first decrease, then increase, become maximum for $x = 0.10$ density, and then decrease. Because of the largest enthalpy with the largest latent heat, the maximum change in the peak position is found for the K−SmA transition. This can be explained in terms of a surface interaction between the aerosil nanoparticles and the 8CB molecules.

B. IR: Molecular Interaction. IR spectroscopy shows the unique absorption characteristics of the functional groups present in the bulk 8CB liquid crystal and aerosil. The effect of the aerosil present in the bulk 8CB can be monitored easily using IR. In the presence of aerosil nanoparticles, bulk 8CB shows an additional strong broad peak for Si−O bonds, as shown in Figure 14. This intense and broad peak at 1082 cm^{-1} is characteristic for Si−O−Si bonds.[42,43] All other peaks in the spectrum of the aerosil and 8CB are found at positions identical to those observed in the IR spectrum of pure 8CB. These results indicate that 8CB has not changed chemically by reacting with aerosil particles, but some surface interaction takes place between aerosil nanoparticles and 8CB molecules due to some weaker force such as hydrogen bonding. As aerosil nanoparticles are added to the bulk 8CB, the position of the peak for the Si−O bonds shifts toward higher frequencies relative to the pure Si−O aerosil nanoparticle. The maximum shift of 28 cm^{-1} in the position of the peak for the Si−O bonds is observed for a density of 0.10 and is toward a higher frequency relative to that of the

TABLE 1: Variation of Activation Energy in the System for Each Transition[a]

system	density (x)	ΔE_{K-A}	ΔE_{A-N}	ΔE_{N-I}
LC_1Sil_0	0.00	1.59	3.43	3.27
$LC_{0.95}Sil_{0.05}$	0.05	0.99	4.29	2.92
$LC_{0.90}Sil_{0.10}$	0.10	0.88	4.93	3.66
$LC_{0.85}Sil_{0.15}$	0.15	0.83	4.67	4.89
$LC_{0.80}Sil_{0.20}$	0.20	1.06	5.41	4.38
LC_0Sil_1	1.00			

[a] Shown are the system, varied with density (system), density of aerosil nanoparticles (density) (in g/cm^3), activation energy for the K−A transition (ΔE_{K-A}) (in jJ mol^{-1}), activation energy for the A−N transition (ΔE_{A-N}) (in kJ mol^{-1}), activation energy for the N−I transition (ΔE_{N-I}) (in kJ mol^{-1}). Errors found in ΔE_{K-A}, ΔE_{A-N}, and ΔE_{N-I} are ± 0.10, ± 0.05, and ± 0.03 kJ/mol, respectively.

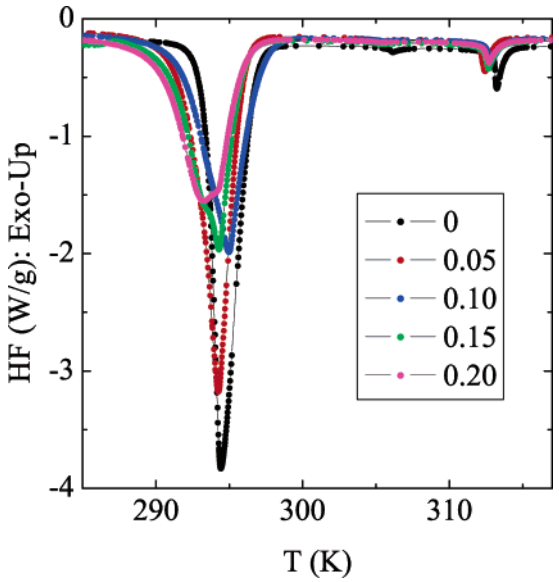

Figure 9. Density dependence shown as a heat flow (W/g) versus temperature (K) plot for all densities of aerosil including bulk 8CB at one heating ramp rate of 5 K/min on a heating scan.

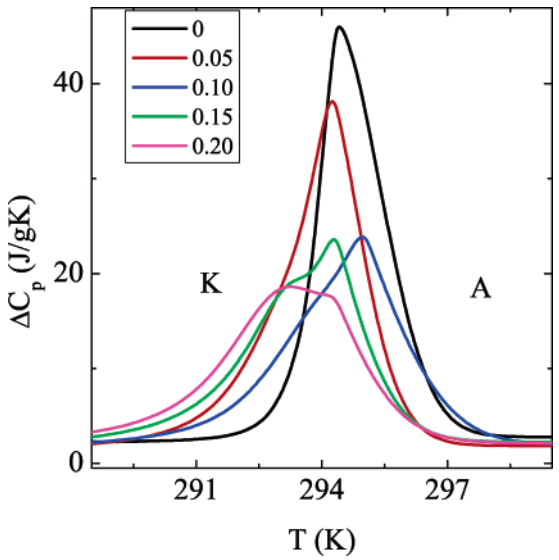

Figure 10. Blow up of the K−SmA transition for all densities at the 5 K/min heating ramp rate plotted as the excess of the specific heat capacity (J/g K) versus temperature (K).

pure Si−O aerosil nanoparticle. Smaller shifts toward higher frequency also are observed for positions of the Si−O peak at higher concentrations of aerosil nanoparticles in 8CB, with the magnitude of the shift decreasing as a function of increasing concentration of aerosil nanoparticles. For example, at a density of 0.20 nanoparticles, the Si−O peak shifted by just 10 cm^{-1} relative to the shift for pure $Si-O_2$. This trend indicates that the shift of the Si−O peak will continue to decrease at increasingly higher concentrations of aerosil nanoparticles in 8CB until a threshold is reached where the Si−O peak of the sample is identical to that observed in pure aerosil nanoparticles, as shown in Figure 15. Peaks corresponding to other functional groups present in the structure of 8CB show no significant change in their positions in the presence of aerosil nanoparticles at the concentrations we examined. Peak positions for the various functional groups on aerosil nanoparticles, 8CB, and the $LC_{1-x}Sil_x$ system are given in the Table 3.

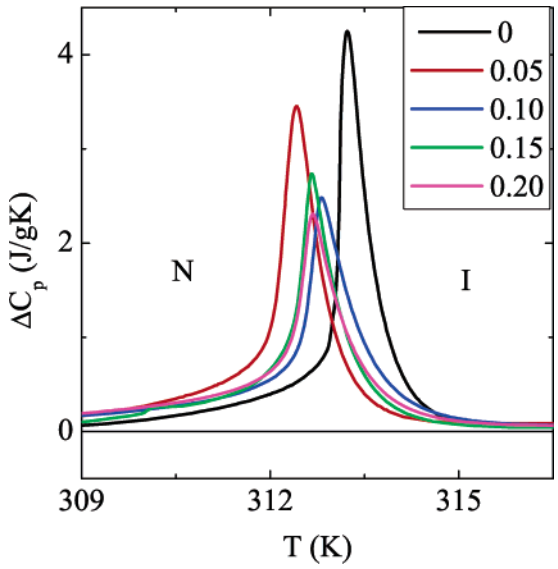

Figure 11. Blow up of the N−I transition for all densities at a 5 K/min heating ramp rate plotted as the excess of the specific heat capacity (J/g K) versus temperature (K).

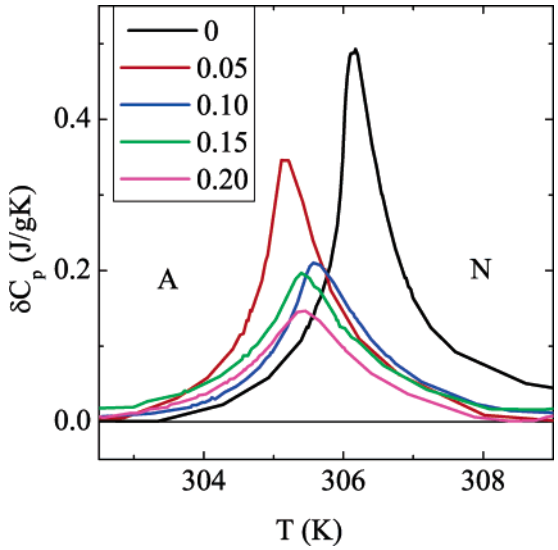

Figure 12. Blow up of the SmA−N transition for all densities at a 5 K/min heating ramp rate plotted as the excess of the specific heat capacity (J/g K) versus temperature (K).

IV. Discussion and Conclusions

A. Discussion on Activated Kinetics. The presence of aerosil nanoparticles in bulk 8CB brings about a molecular disorder and changes the activated kinetics of each transition that can

TABLE 2: Summary of Enthalpy Details with Density Variation in the System[a]

system	density (x)	ΔH_{K-A}	ΔH_{A-N}	ΔH_{N-I}
LC_1Sil_0	0.00	26.91	0.16	0.91
$LC_{0.95}Sil_{0.05}$	0.05	52.90	0.14	1.37
$LC_{0.90}Sil_{0.10}$	0.10	58.30	0.10	1.17
$LC_{0.85}Sil_{0.15}$	0.15	62.59	0.11	0.96
$LC_{0.80}Sil_{0.20}$	0.20	55.96	0.07	0.97
LC_0Sil_1	1.00			

[a] Here are shown the system (system), the density of aerosil nanoparticles (density) (in g/cm^3), the enthalpy for the K−A transition (ΔH_{K-A}) (in kJ mol^{-1}), the enthalpy for the A−N transition (ΔH_{A-N}) (in kJ mol^{-1}), and the enthalpy for the N−I transition (ΔH_{N-I}) (in kJ mol^{-1}). Errors found in ΔH_{K-A}, ΔH_{A-N}, and ΔH_{N-I} are ±1.00, ±0.05, and ±0.10 kJ/mol, respectively.

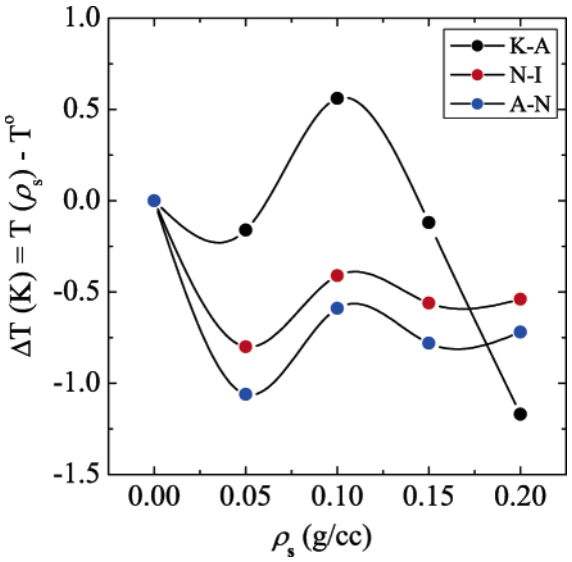

Figure 13. Change in peak positions versus density plot for all transitions at a 5 K/min ramp rate.

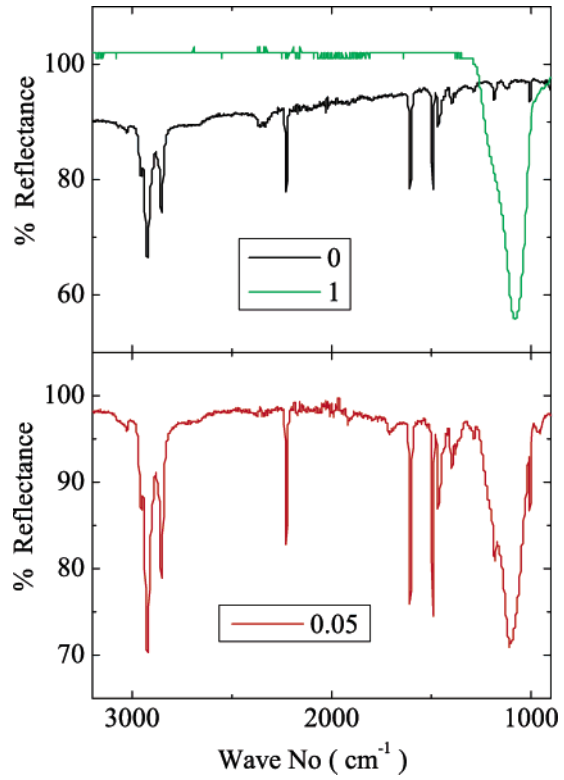

Figure 14. IR results, percent reflectance versus wavenumber (cm^{-1}) plot for the system. The upper panel shows the results of bulk 8CB and bulk aerosil nanoparticles, and the lower panel shows the results of the 0.05 density of aerosil nanoparticles in the system.

be explained using the rate-dependent Arrhenius theory. Using this theory, the activation energy of the transitions can be calculated by the slope obtained from the graph plotted between ln β and $1/T$ in Figures 6, 7, and 8. This energy represents the ordered−disordered molecular motion and rearrangement of the $LC_{1-x}Sil_x$ system near the transition temperature.[37−40] The change in the activation energy of the transitions shows a relationship with their respective enthalpies and can be compared with those for all transitions with density variation (as explained in our earlier publication for bulk 8CB).[36]

Figure 16 shows a comparative plot between the enthalpy and the activation energy of the system for all densities of the

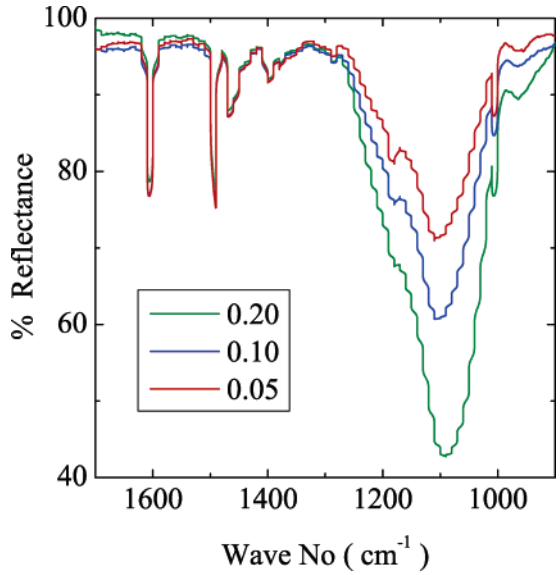

Figure 15. IR results plotted as the percent reflectance versus wavenumber (cm^{-1}) for three densities of the system.

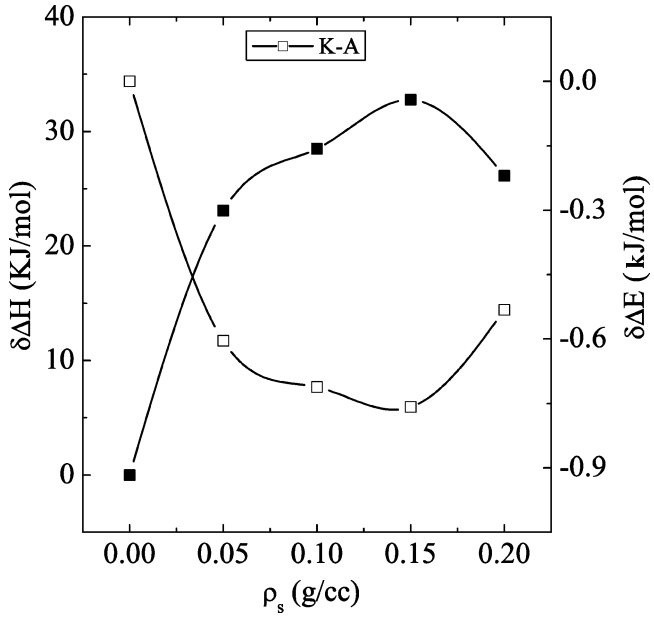

Figure 16. Comparative results of the enthalpy and the activation energy for the K−SmA transition for all densities, where $\delta\Delta H$ and $\delta\Delta E$ can be calculated as $\delta\Delta H$ (kJ/mol) = $\Delta H(\rho_s) - \Delta H°$ and $\delta\Delta E$ (kJ/mol) = $\Delta E(\rho_s) - \Delta E°$. Filled and empty symbols represent the enthalpy and the activation energy for the K−SmA transition, respectively.

K−SmA transition. The data are plotted as a change in the excess of the enthalpy versus density on the left-hand side and as a change in the excess of the activation energy versus density on the right-hand side. Here $\delta\Delta H$ and $\delta\Delta E$ can be calculated as $\delta\Delta H$(kJ/mol) = $\Delta H(\rho_s) - \Delta H°$ and $\delta\Delta E$(kJ/mol) = $\Delta E(\rho_s) - \Delta E°$, where ΔH and ΔE represent the excess in enthalpy and activation energy obtained after subtracting a baseline, respectively. The $\Delta H(\rho_s)$ and $\Delta E(\rho_s)$ are the enthalpies and the activation energies of the system for different densities, and $\Delta H°$ and $\Delta E°$ are the enthalpy and the activation energy for bulk 8CB, respectively. This plot shows that, as the density of the aerosil nanoparticles increases in the system, the enthalpy for the K−SmA transition increases in a pattern, and its respective activation energy decreases in the same pattern. The presence of aerosil nanoparticles in bulk 8CB creates a random disorder

TABLE 3: Summary of IR Results Showing the Positions of the Functional Groups of the Bulk 8CB Liquid Crystal and the Aerosil-Dispersed $LC_{1-x}Sil_x$ System[a]

system	density (x)	phenylrings	C−H	C−N	Si−O
LC_1Sil_0	0.00	2924.1	2853.5	2225.8	
$LC_{0.95}Sil_{0.05}$	0.05	2923.8	2853.3	2226.2	1107.8
$LC_{0.90}Sil_{0.10}$	0.10	2923.8	2853.2	2225.8	1109.2
$LC_{0.80}Sil_{0.20}$	0.20	2923.8	2853.1	2226.0	1091.6
LC_0Sil_1	1.00				1081.7

[a] Shown are the system (system), the density of aerosil nanoparticles (density) (in g/cm^3), the peak position (in cm^{-1}) for phenyl rings, C−H, C−N, and Si−O functional groups (phenylrings, C−H, C−N, and Si−O, respectively).

that causes the system to absorb more energy to go through the melting transition. Hence, the system undergoes an increase in enthalpy as the density of the aerosil nanoparticle increases. This behavior indicates a strong first-order transition that contains a maximum latent heat and hence needs less activation energy for the transition.

Figure 17 shows a comparative plot between the enthalpy and the activation energy for the N−I transition. As the density increases in the system, the enthalpy for the K−SmA transition first increases and then decreases. The respective activation energy shows a decrease and then an increase in the same pattern. The N−I transition is a weak first-order transition containing less latent heat than the K−SmA transition; hence, the N−I transition shows an increase in enthalpy for the lowest density, but after that, it decreases with an increase in the activation energy. The change in activation energy is found to be larger than that for the K−SmA transition because the N−I transition contains less latent heat than the melting transition.

Figure 18 shows a comparative plot between the enthalpy and the activation energy for the SmA−N transition. This transition is a second-order transition that shows no latent heat with the smallest enthalpy. Hence, as density increases in the system, the enthalpy for the SmA−N transition decreases, and its respective activation energy increases in the same pattern. This transition contains the lowest enthalpy and, hence, needs a maximum activation energy, as shown in Tables 1 and 2.

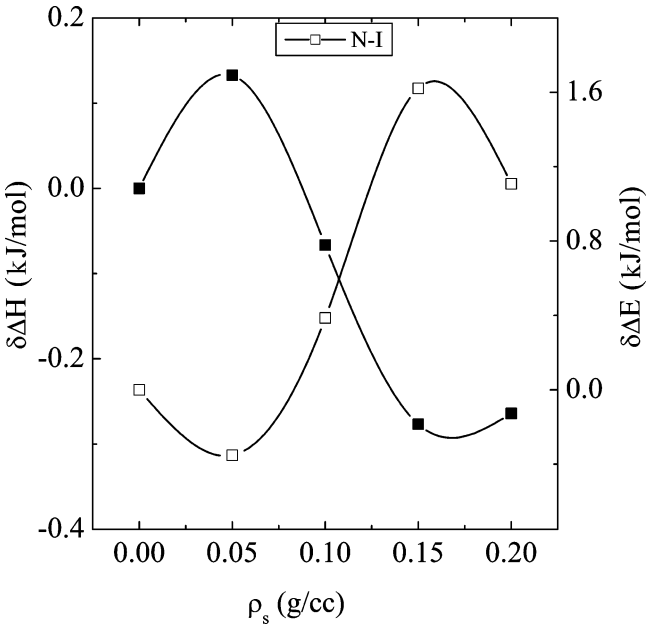

Figure 17. Comparative results of the enthalpy and the activation energy for the N−I transition for all densities. Filled and empty symbols represent the enthalpy and the activation energy for the N−I transition, respectively.

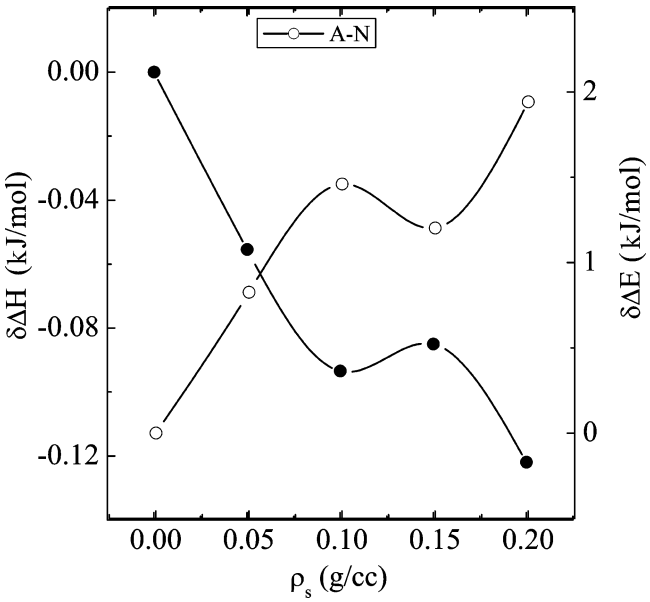

Figure 18. Comparative results of the enthalpy and the activation energy for the SmA−N transition for all densities. Empty and filled symbols represent the enthalpy and the activation energy for the SmA−N transition, respectively.

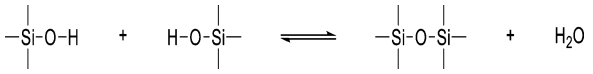

Figure 19. Illustration of how a reaction between surface exposed Si−O−H groups can lead to the formation of Si−O−Si bonds.

B. Discussion on Molecular Disorder. In the presence of aerosil nanoparticles, the most notable feature in the IR spectra is a shift to higher wavenumbers in the frequency for the intense, broad peak corresponding to the Si−O−Si bonds. The Si−O−Si peaks appear at 1108, 1109, and 1092 cm^{-1} in the spectra of samples containing $x = 0.05$, 0.10, and 0.20 in the system, respectively. The magnitude of the shift appears to correlate with the relative percent of aerosil SiO_2 nanoparticles present in the system, with the greatest shift (28 cm^{-1}) occurring in the sample with the 0.10% of aerosil particles and the lowest shift (10 cm^{-1}) occurring in the sample with the highest percent (0.20) of the system. This trend of increasing shift in the position of the Si−O−Si peak as a function of decreasing concentration of aerosil nanoparticles can be explained based on the relative amount of interaction between particles at different relative concentrations. As aerosil nanoparticles are added in 8CB, aerosil nanoparticles form a contact with the 8CB molecules and get coated with them. Aerosil nanoparticles will have the largest amount of contact with the 8CB molecules but the least amount of contact with other aerosil particles at the lowest concentration. They will have an increasing amount of contact with other aerosil nanoparticles as the concentration of the particles increases. For example, individual aerosil nanoparticles dispersed in the system with the lowest density generally will be isolated from other particles and will be coated completely with 8CB. In contrast, individual aerosil nanoparticles dispersed in the system with the highest density should have a significantly higher incidence of contact with other aerosil nanoparticles. As shown in Figure 19, acidic Si−O−H groups exposed on the surface of bulk aerosil can react to form Si−O−Si bonds. Formation of Si−O−Si bonds between aerosil nanoparticles therefore should increase as a function of contact between aerosil nanoparticles. Accordingly, at higher concentrations of aerosil nanoparticles, formation of Si−O−Si bonds between individual particles should lead to the formation of larger particles with a

lower surface to volume ratio than the original, individual SiO_2 particles. A decrease in the surface to volume ratio will lead to a corresponding decrease in the number of surface-exposed Si−O−H groups. Considering that Si−O bonds absorb IR radiation at slightly higher frequencies than Si−O−Si bonds, IR spectra for the lowest density of aerosil nanoparticles should feature peaks for Si−O/Si−O−Si bonds shifted to higher frequencies. Conversely, IR spectra for higher densities of aerosil nanoparticles should feature peaks for Si−O/Si−O−Si bonds at increasingly lower frequencies, with a lower limit of 1082 cm^{-1} (pure aerosil).

The significant change in the position of the Si−O−Si peak indicates that the aerosil nanoparticles (7 nm in diameter) create a disorder between 8CB molecules and shows an interaction with the molecules of liquid crystals (2 nm in size). The aerosil nanoparticles are coated with the 8CB molecules, creating a disorder in the system; hence, it shows a shift toward higher frequencies. As the density of the aerosil nanoparticles starts increasing, the interaction between aerosil nanoparticles and liquid crystal molecules starts decreasing, while their self-interaction increases. The Si−O−Si bond shows a shift toward lower frequencies with the increase in the density as the formation of the Si−O−Si bonds occurs between particles. This behavior can be explained in terms of the order of transition. The K−SmA transition is the strong, first-order transition and contains the largest latent heat; hence, this transition shows a larger disorder in the system with the largest corresponding change in the enthalpy pattern and needs the lowest activation energy. The weaker, first-order transition, N−I, on the other hand, shows a smaller change in the enthalpy and requires a larger activation energy. The second-order transition shows the smallest change in enthalpy and requires the largest change in the activation energy. The maximum change in the position of the Si−O−Si peak is found for 0.10 density; hence, the peak position of each transition shows a maximum change at this density when plotted as the peak position of the transition versus the density, as shown in Figure 13.

C. Conclusions. To understand the role of aerosil dispersion in the $LC_{1-x}Sil_x$ system, the thermodynamic study of activated transitions of the aerosil-dispersed, bulk 8CB system is performed using DSC and IR. DSC shows well-defined endothermic peaks in the heating scan along with an exothermic peak. As the density of the aerosil nanoparticles increases, peaks found on each transition show a temperature shift compared to that of the bulk 8CB results. The peak of each transition becomes smaller and broader in the presence of aerosil nanoparticles. The rate-dependent study shows a significant temperature shift toward lower temperatures, with the decrease in ramp rates for all densities of aerosils following the Arrhenius behavior, and provides the energy dynamics of the $LC_{1-x}Sil_x$ system. The change in enthalpy follows a pattern having a relationship with the respective activation energies and shows activated dynamics for each transition with an increase in the aerosil nanoparticles in the $LC_{1-x}Sil_x$ system, which can be explained in terms of the order of the transition or the latent heat present in the transitions. The strong, first-order transition, K−SmA, contains a maximum latent heat with the largest enthalpy (32.7 kJ mol^{-1}) and hence needs the least activation energy (0.8 kJ mol^{-1}), whereas the weaker, first-order transition, N−I, has a minimum latent heat with an intermediate enthalpy (0.3 kJ mol^{-1}); hence, it requires an intermediate change in activation (1.8 kJ mol^{-1}). The second-order transition, SmA−N, has no latent heat with the smallest enthalpy (0.1 kJ mol^{-1}); hence, this requires a maximum activation energy (2 kJ mol^{-1}). In the presence of aerosil nanoparticles, as the density of aerosil nanoparticles increases in the system, each transition follows a pattern for the change in enthalpies and activation energies, which are found to be exactly opposite to each other, and indicates that the system requires a lesser activation energy as its absorbed energy increases. The change in patterns depends on the interaction between aerosil nanoparticles and 8CB molecules. The significant shift of 28 cm^{-1} in the position of the Si−O−Si peaks shows the greatest interaction between aerosil nanoparticles and 8CB molecules using IR technique. The presence of aerosil nanoparticles in the system creates a random disorder between liquid crystal molecules. As aerosil nanoparticles are added into bulk 8CB, a surface interaction takes place between molecules, where aerosil particles are found to be coated with 8CB molecules and interact with each other under a weak, hydrogen bond interaction. As the density of the aerosil nanoparticles increases in the system, the interaction becomes maximum for 0.10 density of aerosil in the system; hence, it shows a maximum change in the peak position for all transitions as the density of the aerosil increases in the system. As density further increases, the self-interaction between aerosil nanoparticles increases due to formation of Si−O−Si bonds and increases the disorder in the system. This indicates an increase in the enthalpy and a decrease in the activation energy for all transitions as the density of aerosil nanoparticles increases in the system.

Acknowledgment. This work was supported by the NSF-CAREER award DMR-0092786.

References and Notes

(1) Zhou, B.; Iannacchione, G. S.; Garland, C. W.; Bellini, T. *Phys. Rev. E* **1997**, *55*, 2962.
(2) Haga, H.; Garland, C. W. *Phys. Rev. E* **1997**, *56*, 3044.
(3) Bellini, T.; Clark, N. A.; Degiorgio, V.; Mantegazza, F.; Natale, G. *Phys. Rev. E* **1998**, *57*, 2996.
(4) Hourri, A.; Bose, T. K.; Thoen, J. *Phys. Rev. E* **2001**, *63*, 051702.
(5) Marinelli, M.; Ghosh, A. K.; Mercuri, F. *Phys. Rev. E* **2001**, *63*, 061713.
(6) Bellini, T.; Radzihovsky, L.; Toner, J.; Clark, N. A. *Science* **2001**, *294*, 1074.
(7) Retsch, C.; McNulty, I.; Iannacchione, G. S. *Phys. Rev. E* **2002**, *65*, 032701.
(8) Jamee, P.; Pitsi, G.; Thoen, J. *Phys. Rev. E* **2002**, *66*, 021707.
(9) Roshi, A.; Barjami, S.; Paterson, D.; McNulty, I.; Iannacchione, G. S. *Phys. Rev. E*, submitted for publication.
(10) Jin, T.; Finotello, D. *Phys. Rev. Lett.* **2001**, *86*, 818.
(11) Fehr, C.; Dieudonne, P.; Sauvajol, J. L.; Anglaret, E. *Phys. Rev. E* **2003**, *67*, 061706.
(12) Lechner, B.; Marlowe, F.; Nester, E.; Tults, J. *Proc. IEEE* **1971**, *59*, 1566.
(13) Shima, T.; Okumura, M.; Higuchi, T. *Electronics Commun. Jpn., Part II* **1996**, *79*, 73.
(14) Cheng, H.; Gao, H. *J. Appl. Phys.* **2000**, *87*, 7476.
(15) Kawamoto, H. *Proc. IEEE* **2002**, *90*, 460.
(16) Yu, C. C.; Carruzzo, H. M. *Phys. Rev. E* **2004**, *69*, 051201.
(17) Mita, S.; Kondo, S. *Mol. Cryst. Liq. Cryst.* **1986**, *140*, 153.
(18) Leheny, R. L.; Park, S.; Birgeneau, R. J.; Gallani, J. L.; Garland, C. W.; Iannacchione, G. S. *Phys. Rev. E* **2003**, *67*, 011708.
(19) Nozaki, R.; Bose, T. K.; Yagihara, S. *Phys. Rev. A* **1992**, *46*, 7733.
(20) Kosslick, H.; Carius, H.; Frunza, S.; Frunza, L.; Landmesser, H.; Richter, M.; Schreier, S.; Steinike, U.; Fricke, R. *Microporous Mesoporous Mater.* **1998**, *21*, 467.
(21) Scudieri, F.; Marinelli, M.; Zammit, U.; Martellucci, S. *J. Phys. D: Appl. Phys.* **1987**, *20*, 1045.
(22) Iannacchione, G. S.; Garland, C. W.; Mang, J. T.; Rieker, T. P. *Phys. Rev. E* **1998**, *58*, 5966.
(23) Sharma, D.; Iannacchione, G. S. *J. Chem. Phys.*, submitted for publication.
(24) Barjami, S.; Roshi, A.; Sharma, D.; Iannacchione, G. S. *Rev. Sci. Instrum.*, submitted for publication.
(25) Sharma, D.; Mandal, A.; Arguello, J.; Iannacchione, G. S. *Biophys. J.*, to be submitted.
(26) Sharma, D.; Shukla, R.; Singh, A.; Nagpal, A.; Kumar, A. *Adv. Mater. Opt. Electron.* **2000**, *10*, 251.

(27) Ernst, C. R.; Schneider, G. M.; Weiflog, W. *Ber. Bunsen-Ges. Phys. Chem.* **1998**, *102*, 1870.

(28) Donth, E.; Korus, J.; Hempel, E.; Beiner, M. *Thermochim. Acta* **1997**, *305*, 239.

(29) Sharma, D.; Shukla, R.; Kumar, A. *Thin Solid Films* **1999**, *357*, 214.

(30) Degussa Corp., Silica Division, 65 Challenger Road, Ridgefield Park, NJ 07660. Technical data is given in the Degussa booklet Aerosila.

(31) Clegg, P. S.; Stock, C.; Birgeneau, R. J.; Garland, C. W.; Roshi, A.; Iannacchione, G. S. *Phys. Rev. E* **2003**, *67*, 021703.

(32) Clegg, P. S.; Birgeneau, R. J.; Park, S.; Garland, C. W.; Iannacchione, G. S.; Neubert, M. E. *Phys. Rev. E* **2003**, *68*, 031706.

(33) Thoen, J.; Marynissen, H.; Dael, W. V. *Phys. Rev. A* **1982**, *26*, 2886.

(34) A property of certain gels to become fluid when mechanically disturbed (as by shaking or stirring) then resetting after a period of time.

(35) Bellini, T.; Buscaglia, M.; Chiccoli, C.; Mantegazza, F.; Pasini, P.; Zannoni, C. *Phys. Rev. Lett.* **2000**, *85*, 1008.

(36) Sharma, D.; MacDonald, J. C.; Iannacchione, G. S., *J. Phys. Chem. B* **2006**, *110*, 16679.

(37) Vogel, H. *Phys. Z.* **1921**, *22*, 645.

(38) Fulcher, G. S. *J. Am. Ceram. Soc.* **1926**, *6*, 339.

(39) Manaila-Maximean, D.; Rosu, C.; Yamamoto, T.; Yokoyama, H. *Mol. Cryst. Liq. Cryst.* **2004**, *417*, 215.

(40) Blum, F.; Padmanabhan, A.; Mohebbi, R. *Langmuir* **1985**, *1*, 127.

(41) Sharma, D.; Iannacchione, G. S. *J. Phys. Chem. B*, to be submitted.

(42) Sui, R.; Rizkalla, A. S.; Charpentier, P. A. *J. Phys. Chem. B* **2004**, *108*, 11886.

(43) Jackson K. D. O. *Int. J. Vib. Spectrosc.* **1998**, *2*, 69.